

Communication

The Depairing Current Density of a Fe(Se,Te) Crystal Evaluated in Presence of Demagnetizing Factors

Armando Galluzzi ^{1,2}, Krastyo Buchkov ³, Vihren Tomov ³, Elena Nazarova ³, Antonio Leo ^{1,2},
Gaia Grimaldi ², Adrian Crisan ^{4,*} and Massimiliano Polichetti ^{1,2,*}

¹ Department of Physics “E.R. Caianiello”, University of Salerno, Via Giovanni Paolo II, 132, I-84084 Fisciano, Salerno, Italy; agalluzzi@unisa.it (A.G.); aleo@unisa.it (A.L.)

² CNR-SPIN Salerno, Via Giovanni Paolo II, 132, I-84084 Fisciano, Salerno, Italy; gaia.grimaldi@spin.cnr.it

³ Institute of Solid State Physics, Bulgarian Academy of Sciences, 72 Tzarigradsko Chaussee, 1784 Sofia, Bulgaria; buchkov@issp.bas.bg (K.B.); vixren@gmail.com (V.T.); nazarova@issp.bas.bg (E.N.)

⁴ National Institute of Materials Physics, 405A Atomistilor Str., 077125 Magurele, Romania

* Correspondence: adrian.crisan@infim.ro (A.C.); mpolichetti@unisa.it (M.P.)

Abstract: The effect of the demagnetizing factor, regarding the determination of the de-pairing current density J_{dep} , has been studied in the case of a Fe(Se,Te) crystal, using DC magnetic measurements as a function of a magnetic field (H) at different temperatures (T). First, the lower critical field $H_{c1}(T)$ values were obtained, and the demagnetization effects acting on them were investigated after calculating the demagnetizing factor. The temperature behaviors of both the original H_{c1} values and the ones obtained after considering the demagnetization effects (H_{c1}^{demag}) were analyzed, and the temperature dependence of the London penetration depth $\lambda_L(T)$ was obtained in both cases. In particular, the $\lambda_L(T)$ curves were fitted with a power law dependence, indicating the presence of low-energy quasiparticle excitations. Furthermore, by plotting λ_L^{-2} as a function of T , we found that our sample behaves as a multigap superconductor, which is similar to other Fe-11 family iron-based compounds. After that, the coherence length ξ values were extracted, starting with the $H_{c2}(T)$ curve. The knowledge of λ_L and ξ allowed us to determine the J_{dep} values and to observe how they are influenced by the demagnetizing factor.

Keywords: de-pairing current density; demagnetizing factor; demagnetization effects; iron-based superconductors; lower critical field; London penetration depth; coherence length; magnetism and superconductivity



Citation: Galluzzi, A.; Buchkov, K.; Tomov, V.; Nazarova, E.; Leo, A.; Grimaldi, G.; Crisan, A.; Polichetti, M. The Depairing Current Density of a Fe(Se,Te) Crystal Evaluated in Presence of Demagnetizing Factors. *Condens. Matter* **2023**, *8*, 91. <https://doi.org/10.3390/condmat8040091>

Academic Editors: Ali Gencer, Annette Bussmann-Holder, J. Javier Campo Ruiz, Valerii Vinokur and Germán F. de la Fuente

Received: 27 September 2023

Revised: 20 October 2023

Accepted: 20 October 2023

Published: 23 October 2023



Copyright: © 2023 by the authors. Licensee MDPI, Basel, Switzerland. This article is an open access article distributed under the terms and conditions of the Creative Commons Attribution (CC BY) license (<https://creativecommons.org/licenses/by/4.0/>).

1. Introduction

The initial discovery of superconductivity in fluorine-doped LaFeAsO [1] attracted a lot of interest in the scientific community. Nevertheless, it was an iron-based superconductor, but with oxygen in its stoichiometric formula. This prompted us to correlate this compound with previously discovered cuprates superconductors [2]. Later, with the important discovery of the $Ba_{1-x}K_xFe_2As_2$ compound, it became clear that the importance of this new class of materials (which can present not-oxide superconductors) breaks the link with cuprates. This highlights the fact that, for fabricating high-temperature superconductors, oxygen does not necessary play a crucial role. The 11 family in the class of iron-based superconductors has been intensively investigated in recent years so that we may understand the basic mechanism governing its superconductivity [3]. These materials have a layered structure, like cuprates, and they show interesting peculiarities such as high values in the upper critical field, critical current density, and irreversibility field [4–7]. Moreover, they have lower anisotropy values than cuprates, with associated high pinning energy values [8–11]. Among these properties, there are also non-monotonic responses to magnetization with applied magnetic fields; this has led to particular phenomena that have been deeply studied in recent years [12–16]. These phenomena are strictly correlated

with vortex dynamics [17–21]. On the other hand, the presence of vortices inside type-II superconductors can also be investigated by analyzing the lower critical field, H_{c1} , together with the London penetration depth, λ_L . H_{c1} and λ_L are useful parameters for gathering information regarding the bulk thermodynamic properties of a sample, and they have been investigated for iron-based compounds in the past [22–24]. In particular, compared with other physical quantities, penetration depth is a useful parameter to study the superconductivity of a compound intrinsically; this is because it is not sensitive to the aspects related to surface conditions. In particular, the study of the behavior of λ_L^{-2} , as a function of temperature, can provide information on the superconductivity typology characterizing the sample (e.g., single gap BCS theory, the two gap model, etc.) [25–27]. Moreover, the λ_L values indicate the strength of the interactions between vortices, thus allowing us to deduce the magnitude of the effective pinning energy of the sample. λ_L , together with the coherence length, ξ , represent the fingerprints of a superconductor, and this study becomes crucial when first characterizing a new superconductor. Moreover, by combining them, it is possible to obtain the de-pairing current density, J_{dep} , which fixes the upper limit of the presence of superconductivity inside a superconducting material. The de-pairing current density is of significant importance for understanding the existing limits for increasing J_c [28,29], and since it directly provides data on the critical velocity of the superfluid, it is essential for the investigation of the superconducting mechanism and the symmetry of the superconducting gap [30]. Using this framework, by following the Ginzburg–Landau theory, the de-pairing current density, J_{dep} , depends on the characteristic critical parameters H_{c1} and H_{c2} , and more specifically, the London penetration depth, λ_L , and the coherence length, ξ [30,31]. In this work, the influence of the demagnetization effects on the de-pairing current density, J_{dep} , has been analyzed by studying a Fe(Se,Te) iron-based superconductor. We started by measuring the first magnetization curve at different temperatures in order to obtain the lower critical field H_{c1} values. We have noted that the demagnetization effects acting on the sample were significant, and they resulted in an underestimation of the real H_{c1} values. From the H_{c1} values, the London penetration depth, λ_L , as a function of the temperature, was obtained, and it was noted that it is not possible to fit the penetration depth with the typical exponential behavior that characterizes the s-wave superconductor. In this context, the plot of λ_L^{-2} , as a function of T , confirmed that our sample shows peculiarities which can be ascribed to a multigap superconducting behavior. Finally, after determining the coherence length, ξ , from the upper critical field, H_{c2} , the J_{dep} values were calculated as a function of the temperature, by considering the demagnetization effects and not considering them; this provided very high values in the framework of the iron-based superconductors.

2. Results and Discussion

In order to study the lower critical field, H_{c1} behavior, as a function of temperature T , the virgin magnetic moment vs. magnetic field was measured at different temperatures. In Figure 1, the first branch of the superconducting hysteresis loop was reported as reaching up to 0.3 T in the temperature range of 2.5 K to 10 K. The initial linear decrease of the magnetic moment m was visible due to the Meissner state, and the reduction of the superconducting signal was visible due to the increase in temperature. To determine H_{c1} at a fixed temperature, the first value that deviated from the linear trend of the Meissner state (black dashed line) meaning that the vortices have penetrated the sample building up a critical state [32–34]. Considering all the temperatures, the $H_{c1}(T)$ behavior was obtained and then fitted using the following equation [35]:

$$H_{c1}(T) = H_{c1}(0) \left(1 - \frac{T}{T_c}\right)^n \quad (1)$$

where $H_{c1}(0)$ is the value of H_{c1} at $T = 0$ K, $T_c = 14.5$ K [4], and n is the exponent. As per the fitting procedure, $H_{c1}(0) = 143$ Oe and $n = 1.54$ were obtained. The $H_{c1}(T)$ curve, together with its fit, is presented in Figure 2a (black squares and black solid line). It is worth noting

that the $H_{c1}(T)$ curve shows an upward trend with a negative curvature; this was not predicted in the single-band gap description of the mean-field theory, therefore, it is evident that two energy gaps exist [36]. Generally, a superconductor immersed in a magnetic field is subject to demagnetization effects at low fields due to its finite dimensions [37,38]. Considering that the demagnetization effects are stronger when the sample is in a perpendicular field configuration, these effects cannot be overlooked in our case. In particular, the H_{c1} values are underestimated because, due to the demagnetization effects, the sample experiences a magnetic field higher than the applied one. Therefore, in order to take into account the demagnetization effects acting on the sample, the H_{c1} values must be properly scaled using the so-called demagnetizing factor. More specifically, the demagnetized H_{c1} values (H_{c1}^{demag}), as a function of temperature, were calculated using the formula reported by Yeshurun et al. [39].

$$H_{c1}^{demag} = \frac{H_{c1}}{(1 - N)} \tag{2}$$

where N is the demagnetizing factor which can assume values ranging between 0 and 1. The N value can be determined using the following formula [37,38]:

$$N = \left(\frac{H}{4\pi M} \right) + 1 \tag{3}$$

where M is the magnetization in the Meissner state and H is the applied field. In our case, N has been already estimated to be approximately 0.76 in Ref. [4], which is quite a high value; this aligns with the perpendicular field configuration. Therefore, using Equation (2) with $N = 0.76$, the demagnetized values for H_{c1} were calculated and fitted with the following equation:

$$H_{c1}^{demag}(T) = H_{c1}^{demag}(0) \left(1 - \frac{T}{T_c} \right)^n \tag{4}$$

where $H_{c1}^{demag}(0)$ is the value of H_{c1}^{demag} at $T = 0$ K, $T_c = 14.5$ K [4], and n is the exponent. From the fitting procedure, $H_{c1}^{demag}(0) = 597$ Oe and $n = 1.54$ were obtained. The $H_{c1}^{demag}(T)$ curve, together with its fit, is presented in Figure 2a (red circles and red dashed line).

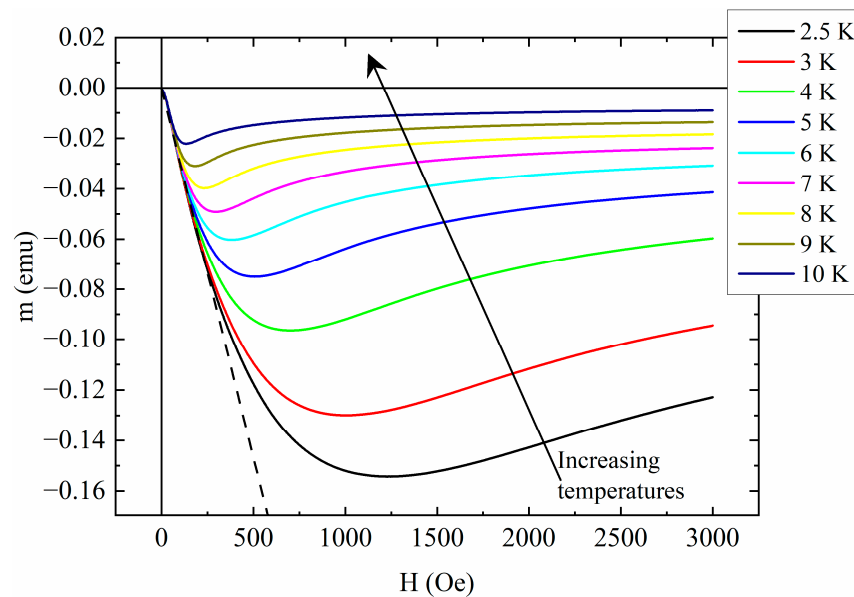


Figure 1. The field dependence of the initial magnetic moment curve is plotted for different temperatures. The black dashed line provides the linear fit for the low field $m(H)$ curves.

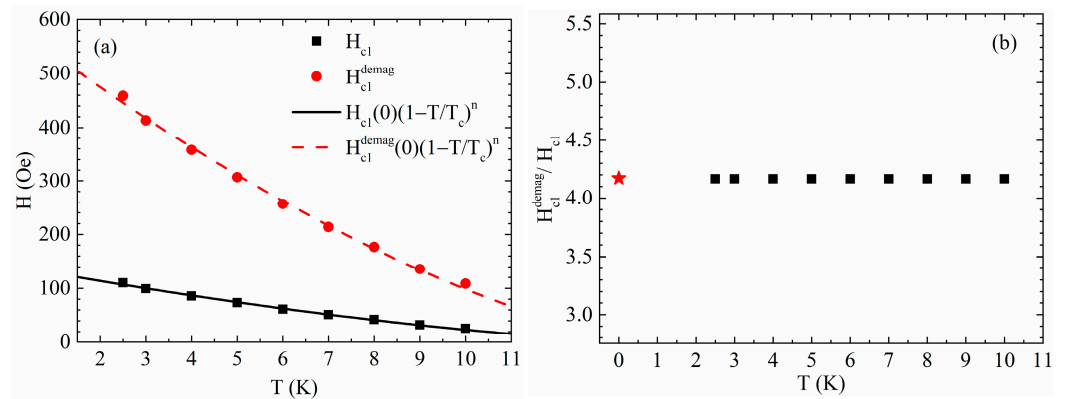


Figure 2. (a) Comparison between the temperature dependence of the lower critical field H_{c1} (black squares) (where the black solid line is the fit of the data using the following equation, $H_{c1}(T) = H_{c1}(0)\left(1 - \frac{T}{T_c}\right)^n$) and the temperature dependence of the lower critical field after considering the demagnetization effects H_{c1}^{demag} (red circles) (where the red dashed line is the fit of the data using the following equation $H_{c1}^{demag}(T) = H_{c1}^{demag}(0)\left(1 - \frac{T}{T_c}\right)^n$). When performing the fit, $H_{c1}(0) = 143$ Oe and $n = 1.54$ were obtained without considering the demagnetizing factor, and $H_{c1}^{demag}(0) = 597$ Oe and $n = 1.54$ were obtained by considering the demagnetizing factor. (b) Ratio of the $H_{c1}^{demag}(T)$ and $H_{c1}(T)$ values. The red star indicates the ratio of $H_{c1}^{demag}(0)/H_{c1}(0)$.

As previously mentioned, the H_{c1}^{demag} values are higher than the H_{c1} ones, as reported in Figure 2a. In Figure 2b, the ratio of the $H_{c1}^{demag}(T)$ and $H_{c1}(T)$ values was reported to show a value equal to approximately four. On the other hand, the $H_{c1}^{demag}(0)/H_{c1}(0)$ value was also reported to be a red star in Figure 2b, and it is still equal to approximately four, thus confirming the viability of the fitting procedures that were previously performed. From the determination of the lower critical field values, the temperature dependence of the London penetration depth, λ_L , can be obtained using the following formula [25]:

$$H_{c1} = \left(\frac{\phi_0}{4\pi\lambda_L^2} \right) \ln k \tag{5}$$

where $\phi_0 = 2.07 \times 10^{-7}$ Oe cm² is the magnetic flux quantum and k is the Ginzburg–Landau parameter. Using the Ginzburg–Landau theory, and by following the approach reported in Ref. [40], k can be calculated using the relation $k = H_{c2}(0)/(2^{1/2}H_c(0))$, where $H_c(0)$ is the thermodynamic critical field. $H_c(0)$ is calculated using H_{c1} , H_{c1}^{demag} , and H_{c2} values at a temperature of zero (i.e., $H_c(0) = (H_{c1}(0) \times H_{c2}(0))^{1/2} \approx 8$ kOe and $H_c^{demag}(0) = (H_{c1}^{demag}(0) \times H_{c2}(0))^{1/2} \approx 16.5$ kOe); therefore, obtaining $k \approx 40$ and $k^{demag} \approx 20$ aligns with other Fe-chalcogenide superconductors [40–43]. For the calculation of λ_L , Equation (5), both H_{c1} and H_{c1}^{demag} , together with the k and k^{demag} values, were used, and the results are reported in Figure 3. Both the $\lambda_L(T)$ curves were fitted using the following equation:

$$\lambda_L(T) = \lambda_L(0) \left(1 - \frac{T}{T_c} \right)^n \tag{6}$$

where $\lambda_L(0)$ is the London penetration depth at $T = 0$ K, $T_c = 14.5$ K [4], and n is the exponent. From the fitting procedure, $\lambda_L(0) = 208$ nm, $n = -0.72$, and $\lambda_L^{demag}(0) = 92$ nm, and $n = -0.72$ were obtained, having considered the H_{c1} , k , and H_{c1}^{demag} , k^{demag} values for the λ_L calculation, respectively. At low temperatures, λ_L does not show the typical exponential behavior expected for a fully gapped clean s -wave superconductor [44]. In

general, a power law temperature dependence of λ_L implies the presence of low-energy quasiparticle excitations [45].

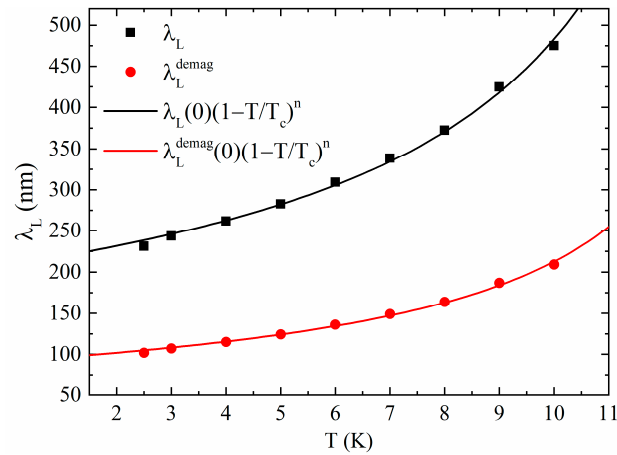


Figure 3. Temperature dependence of the London penetration depth λ_L obtained from H_{c1} (black squares) and H_{c1}^{demag} (red circles). Both the curves were fitted with $\lambda_L(T) = \lambda_L(0)\left(1 - \frac{T}{T_c}\right)^n$. When performing the fit, $\lambda_L(0) = 208$ nm and $n = -0.72$ were obtained without considering the demagnetizing factor, whereas $\lambda_L^{demag}(0) = 92$ nm and $n = -0.72$ were obtained by considering the demagnetizing factor.

In this framework, when plotting λ_L^{-2} as a function of T (see Figure 4), the curve behavior was noted as being completely different from the behavior predicted using the single-gap BCS theory, which should have an opposite concavity; this indicates a more probable multigap superconductivity in our sample [25,27,46,47]. This aligns with the results reported in the literature for Fe-based pnictides [48–51]. On the other hand, it should be noted that the $\lambda_L^{-2}(T)$ curvature may be also a sign that the sample has an anisotropic single gap nature [52]. Finally, it is worth noting that the λ_L^{demag} values obtained from H_{c1}^{demag} appear low in respect to other Fe(Se,Te) samples reported in the literature [45,46,53,54], indicating a low vortex–vortex interaction that, in the framework of vortex dynamics, usually characterizes a single vortex state. This vortex lattice configuration, due to the strength of the effective pinning energy, typically allows the sample to carry high transport currents in high fields that are suitable for power applications of this class of superconducting materials. After the calculation of the λ_L values, the coherence length ξ values were extracted, starting with the $H_{c2}(T)$ curve reported in Figure 12 of Ref. [4], using the following equation [55,56]:

$$H_{c2}(T) = \frac{\phi_0}{2\pi\xi^2(T)} \tag{7}$$

where $\phi_0 = 2.068 \times 10^{-15}$ Tm² is the magnetic flux quantum.

The ξ values, as a function of temperature, are shown in Figure 5 together with the fit with the equation [57]:

$$\xi(T) = \xi(0)\left(1 - \frac{T}{T_c}\right)^n \tag{8}$$

where $\xi(0)$ is the coherence length at 0 K, $T_c = 14.5$ K [4], and n is the exponent. From the fitting procedure, we obtained $\xi(0) \approx 3$ nm, which coheres with the value, $\xi(0) \approx 2.7$ nm, which was calculated using $H_{c2}(0) = 46.5$ T from Ref. [4], and $n \approx -0.64$, from Ref. [57]. The determination of the penetration depth, and the coherence length values, allows us to estimate the de-pairing current density, J_{dep} . The de-pairing current density is the current value above which the superconductivity of the superconductor is completely broken; this is because it is the value wherein the kinetic energy of the superconducting carriers equals

the binding energy of the Cooper pair. The de-pairing current density can be expressed, thanks to the Ginzburg–Landau theory, as follows [30,31]:

$$J_{dep}(T) = \frac{\phi_0}{3^{3/2}\pi\mu_0\lambda_L^2\xi} \tag{9}$$

where μ_0 is the vacuum permeability. It is worth underlining that this equation is usually only considered valid for temperatures approaching T_c . Nevertheless, by taking into account the calculations performed by Bardeen [58], the de-pairing current density deviates from the GL theory by a maximum factor of 1.5 at $T = 0$ K; this indicates that it is possible to study its temperature behavior with reasonable error. Moreover, Equation (9) is usually valid for the single band superconductor, whereas Fe(Se,Te) shows peculiarities which can be ascribed to a multigap superconducting behavior, as previously mentioned. In this context, another important parameter to consider is $\gamma_H = H_{c2,ab}/H_{c2,c}$, and in particular, its temperature dependence. In fact, in a single gap superconductor, the γ_H parameter is temperature independent, while in a multiband superconductor, the contributions of different bands lead to a non-constant γ_H , with each band contributing differently as T is changed. For Fe(Se,Te), it is evident in several works [59–61] that γ_H is slightly dependent on temperature, therefore, making reasonable the use of the GL formula, although it gives overestimated J_{dep} values, especially at low temperatures. The J_{dep} values, obtained using Equation (9), are reported in Figure 6. It is worth noting the presence of two $J_{dep}(T)$ curves. In particular, the black curve was obtained using λ_L without the demagnetization correction, whereas the red curve was obtained by considering λ_L^{demag} in conjunction with the demagnetization correction. Both sets of J_{dep} values align with the highest values reported for the different iron-based families; this demonstrates the very good quality of this crystal [62–66]. It is evident that the J_{dep}^{demag} values that take the demagnetizing factor into account are five times higher than the J_{dep} values obtained without considering the demagnetizing factor. This helps us understand how important the demagnetizing factor is when estimating different important superconducting parameters such as H_{c1} , λ_L , and J_{dep} . It is important to note that the role of λ_L is crucial to Equation (9) since it is squared, and therefore, a small λ_L change generates a large J_{dep} variation. In conclusion, in light of the fact that H_{c1} and λ_L can strongly depend on stoichiometry, the possibility of tuning it by modifying the fabrication process and parameters could be exploited to enhance the de-pairing current density.

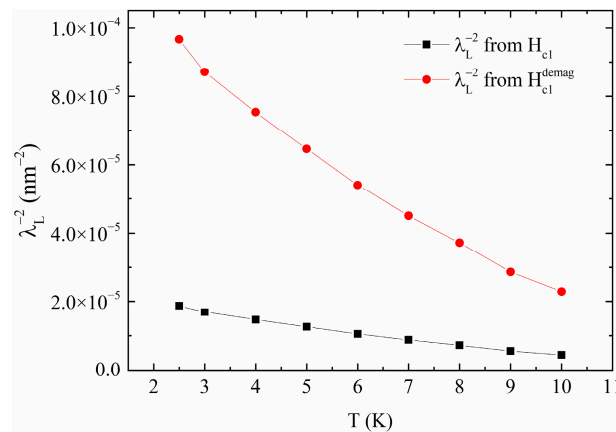


Figure 4. Temperature dependence of the London penetration depth λ_L^{-2} , obtained from H_{c1} (black squares) and H_{c1}^{demag} (red circles). The solid lines are a guide for the eyes.

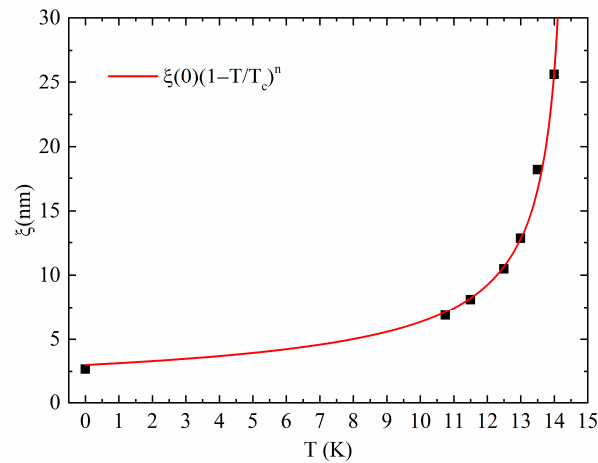


Figure 5. Temperature dependence of the coherence length, ξ (black squares), together with its fit and the following equation $\xi(T) = \xi(0)\left(1 - \frac{T}{T_c}\right)^n$. After performing the fit, $\xi(0) \approx 3$ nm and $n \approx -0.64$ were obtained.

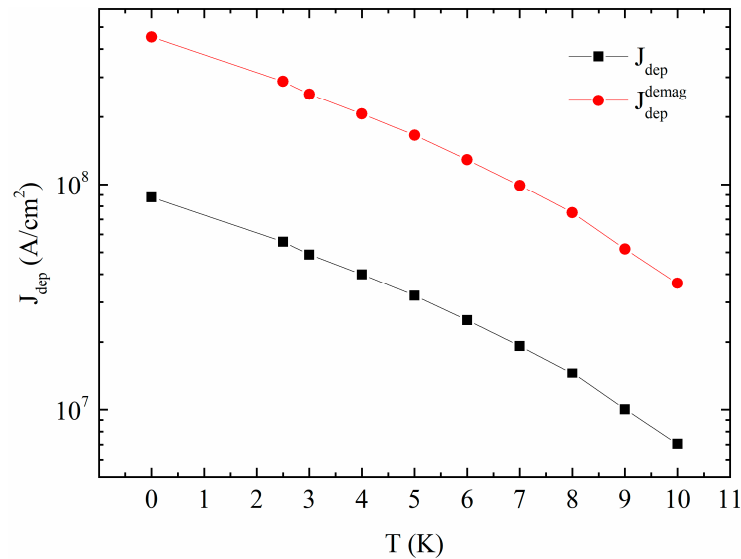


Figure 6. Temperature dependence of the de-pairing current density, J_{dep} with (red closed circles) and without (black closed squares) consideration of the demagnetizing factor. The solid lines are a guide for the eyes.

3. Materials and Methods

We analyzed a $\text{FeSe}_{0.5}\text{Te}_{0.5}$ (nominal composition) crystal with the following dimensions: $3 \times 3 \times 0.2$ mm³. The crystal was created using the Bridgman technique, and $T_c = 14.5$ K. Details concerning the creation of the crystal are reported elsewhere [4]. A SEM-EDX analysis was performed on the sample, which showed the presence of twin boundaries and a slight deviation from the nominal composition in terms of stoichiometry ($\text{Fe}_{0.96}\text{Te}_{0.59}\text{Se}_{0.45}$) [67]. This is probably due to micro inhomogeneity and the phase separation of magnetic premises, which is typical for crystal growth and synthesis in Fe-SeTe [68–70] and its basic compound FeSe [71–73]. The sample was characterized in a dc magnetic field that was applied perpendicularly to its largest face ($H \parallel c$). In particular, the dc magnetic moment, as a function of the field, $m(H)$, was measured using a Quantum Design PPMS-9T equipped with a VSM option. To avoid the effect on the sample response caused by the residual trapped field inside the PPMS dc magnet [74], this field was reduced below 1×10^{-4} T [75]. Regarding the $m(H)$ measurements, the sample was first cooled down to the measurement temperature in the zero field and thermally stabilized for at least

20 min. Then, the field was ramped with the fixed sweep rate value to +9 T, then it was reduced to −9 T, and finally, to +9 T again in order to acquire the complete hysteresis loop.

4. Conclusions

By studying the DC magnetic moment as a function of the magnetic field (H) at different temperatures (T) on a Fe(Se,Te) crystal created using the Bridgman technique, the effect of the demagnetizing factor on the de-pairing current density J_{dep} values was estimated. In order to achieve this, the London penetration depth and the coherence length were evaluated. Initially, the lower critical field, H_{c1} , was obtained as a function of temperature that focused on the impact that demagnetization effects have on its values. In particular, it was found that H_{c1} values were underestimated by a factor equal to four, even at $T = 0$ K. Starting with these results, the London penetration depth, λ_L , was calculated as a function of temperature using both the original H_{c1} values and the values obtained after considering the demagnetization effects (H_{c1}^{demag}). The $\lambda_L(T)$ curves did not show the typical exponential behavior that was expected for a fully gapped clean s -wave superconductor, but rather, they exhibited a power law dependence that indicated the presence of low-energy quasiparticle excitations. In this framework, λ_L^{-2} , as a function of T , was graphed, and multigap-like behavior was found in our sample, which aligns with the behavior of other iron-based samples reported in the literature. Additionally, we found that the λ_L^{demag} values obtained from H_{c1}^{demag} are lower than the values obtained from other Fe(Se,Te) samples reported in the literature, which suggests a possible single vortex state. In this vortex lattice configuration, the effective pinning energy is high, therefore, reducing the dissipations inside the material, and improving the current transport properties is suitable for power applications of this class of superconducting materials. After that, the coherence length ξ values were extracted, starting with the $H_{c2}(T)$ curve, as reported in our previous work. Combining the λ_L and ξ values, the J_{dep} values that took the demagnetization effects into account, as a function of temperature, were five times higher than the values that did not take the demagnetization effects into account. Tuning the stoichiometry of the compounds by modifying the fabrication procedures, and thus, changing the H_{c1} and λ_L values by considering the demagnetizing factor, can push the limits of the de-pairing current density values of the materials.

Author Contributions: Conceptualization, A.G., K.B., V.T. and E.N.; methodology, A.G. and K.B.; software, A.G., V.T. and A.L.; validation, K.B., E.N., G.G. and A.C.; formal analysis, A.G. and K.B.; investigation, A.G. and K.B.; resources, A.C. and M.P.; data curation, A.G., K.B. and V.T.; writing—original draft preparation, A.G.; writing—review and editing, K.B., E.N., G.G., A.C. and M.P.; visualization, K.B., A.L. and G.G.; supervision, A.C. and M.P.; project administration, A.C. and M.P.; funding acquisition, A.C. and M.P. All authors have read and agreed to the published version of the manuscript.

Funding: This work was supported by the EU COST Actions CA19108 Hi-SCALE, CA20116 OPERA and CA21144 SUPERQUMAP. A.C. gratefully acknowledges the funding from the Core Program of the National Institute of Materials Physics, granted by the Romanian Ministry of Research, Innovation, and Digitalization under the Project PC2-PN23080202.

Data Availability Statement: All the data reported are available from the authors upon reasonable request.

Acknowledgments: This work has been carried out within the framework of the inter-academic Italian-Bulgarian research project 2019–2021 (Department of Physics ‘E R Caianiello’ CNR-SPIN unit, University of Salerno and the Institute of Solid State Physics ‘Georgi Nadjakov’, Bulgarian Academy of Sciences). The authors would like to thank M. Gospodinov from ISSP-BAS for the valuable discussions and the support for the sample preparation.

Conflicts of Interest: The authors declare no conflict of interest.

References

1. Kamihara, Y.; Watanabe, T.; Hirano, M.; Hosono, H. Iron-based layered superconductor $\text{La}[\text{O}_{1-x}\text{F}_x]\text{FeAs}$ ($x = 0.05\text{--}0.12$) with $T_c = 26$ K. *J. Am. Chem. Soc.* **2008**, *130*, 3296–3297. [[CrossRef](#)]
2. Bednorz, J.G.; Müller, K.A. Possible high T_c superconductivity in the Ba-La-Cu-O system. *Z. Phys. B Condens. Matter* **1986**, *64*, 189–193. [[CrossRef](#)]
3. Hsu, F.-C.; Luo, J.-Y.; Yeh, K.-W.; Chen, T.-K.; Huang, T.-W.; Wu, P.M.; Lee, Y.-C.; Huang, Y.-L.; Chu, Y.-Y.; Yan, D.-C.; et al. Superconductivity in the PbO-type structure $\alpha\text{-FeSe}$. *Proc. Natl. Acad. Sci. USA* **2008**, *105*, 14262–14264. [[CrossRef](#)] [[PubMed](#)]
4. Galluzzi, A.; Buchkov, K.; Tomov, V.; Nazarova, E.; Leo, A.; Grimaldi, G.; Nigro, A.; Pace, S.; Polichetti, M. Evidence of pinning crossover and the role of twin boundaries in the peak effect in FeSeTe iron based superconductor. *Supercond. Sci. Technol.* **2018**, *31*, 015014. [[CrossRef](#)]
5. Galluzzi, A.; Buchkov, K.; Nazarova, E.; Tomov, V.; Grimaldi, G.; Leo, A.; Pace, S.; Polichetti, M. Transport properties and high upper critical field of a Fe(Se,Te) iron based superconductor. *Eur. Phys. J. Spec. Top.* **2019**, *228*, 725–731. [[CrossRef](#)]
6. Galluzzi, A.; Buchkov, K.; Nazarova, E.; Tomov, V.; Leo, A.; Grimaldi, G.; Pace, S.; Polichetti, M. Magnetic field sweep rate influence on the critical current capabilities of a Fe(Se,Te) crystal. *J. Appl. Phys.* **2020**, *128*, 073902. [[CrossRef](#)]
7. Hosono, H.; Yamamoto, A.; Hiramatsu, H.; Ma, Y. Recent advances in iron-based superconductors toward applications. *Mater. Today* **2018**, *21*, 278–302. [[CrossRef](#)]
8. Yuan, H.Q.; Singleton, J.; Balakirev, F.F.; Baily, S.A.; Chen, G.F.; Luo, J.L.; Wang, N.L. Nearly isotropic superconductivity in $(\text{Ba,K})\text{Fe}_2\text{As}_2$. *Nature* **2009**, *457*, 565–568. [[CrossRef](#)] [[PubMed](#)]
9. Yamamoto, A.; Jaroszynski, J.; Tarantini, C.; Balicas, L.; Jiang, J.; Gurevich, A.; Larbalestier, D.C.; Jin, R.; Sefat, A.S.; McGuire, M.A.; et al. Small anisotropy, weak thermal fluctuations, and high field superconductivity in Co-doped iron pnictide $\text{Ba}(\text{Fe}_{1-x}\text{Co}_x)_2\text{As}_2$. *Appl. Phys. Lett.* **2009**, *94*, 062511. [[CrossRef](#)]
10. Grimaldi, G.; Leo, A.; Martucciello, N.; Braccini, V.; Bellingeri, E.; Ferdeghini, C.; Galluzzi, A.; Polichetti, M.; Nigro, A.; Villegier, J.-C.; et al. Weak or Strong Anisotropy in Fe(Se,Te) Superconducting Thin Films Made of Layered Iron-Based Material? *IEEE Trans. Appl. Supercond.* **2019**, *29*, 1–4. [[CrossRef](#)]
11. Leo, A.; Braccini, V.; Bellingeri, E.; Ferdeghini, C.; Galluzzi, A.; Polichetti, M.; Nigro, A.; Pace, S.; Grimaldi, G. Anisotropy effects on the quenching current of Fe(Se,Te) Thin Films. *IEEE Trans. Appl. Supercond.* **2018**, *28*, 8234633. [[CrossRef](#)]
12. Eley, S.; Willa, R.; Chan, M.K.; Bauer, E.D.; Civale, L. Vortex phases and glassy dynamics in the highly anisotropic superconductor $\text{HgBa}_2\text{CuO}_{4+\delta}$. *Sci. Rep.* **2020**, *10*, 10239. [[CrossRef](#)]
13. Polichetti, M.; Galluzzi, A.; Buchkov, K.; Tomov, V.; Nazarova, E.; Leo, A.; Grimaldi, G.; Pace, S. A precursor mechanism triggering the second magnetization peak phenomenon in superconducting materials. *Sci. Rep.* **2021**, *11*, 7247. [[CrossRef](#)] [[PubMed](#)]
14. Llovo, I.F.; Sónora, D.; Mosqueira, J.; Salem-Sugui, S.; Sundar, S.; Alvarenga, A.D.; Xie, T.; Liu, C.; Li, S.L.; Luo, H.Q. Vortex dynamics and second magnetization peak in the iron-pnictide superconductor $\text{Ca}_{0.82}\text{La}_{0.18}\text{Fe}_{0.96}\text{Ni}_{0.04}\text{As}_2$. *Supercond. Sci. Technol.* **2021**, *34*, 115010. [[CrossRef](#)]
15. Yi, X.; Xing, X.; Meng, Y.; Zhou, N.; Wang, C.; Sun, Y.; Shi, Z. Anomalous Second Magnetization Peak in 12442-Type $\text{RbCa}_2\text{Fe}_4\text{As}_4\text{F}_2$ Superconductors. *Chin. Phys. Lett.* **2023**, *40*, 027401. [[CrossRef](#)]
16. Lopes, P.V.; Sundar, S.; Salem-Sugui, S.; Hong, W.; Luo, H.; Ghivelder, L. Second magnetization peak, anomalous field penetration, and Josephson vortices in $\text{KCa}_2\text{Fe}_4\text{As}_4\text{F}_2$ bilayer pnictide superconductor. *Sci. Rep.* **2022**, *12*, 20359. [[CrossRef](#)]
17. Prozorov, R.; Ni, N.; Tanatar, M.A.; Kogan, V.G.; Gordon, R.T.; Martin, C.; Blomberg, E.C.; Prommaman, P.; Yan, J.Q.; Bud'ko, S.L.; et al. Vortex phase diagram of $\text{Ba}(\text{Fe}_{0.93}\text{Co}_{0.07})_2\text{As}_2$ single crystals. *Phys. Rev. B* **2008**, *78*, 224506. [[CrossRef](#)]
18. Sun, Y.; Taen, T.; Tsuchiya, Y.; Pyon, S.; Shi, Z.; Tamegai, T. Magnetic relaxation and collective vortex creep in $\text{FeTe}_{0.6}\text{Se}_{0.4}$ single crystal. *Europhys. Lett.* **2013**, *103*, 57013. [[CrossRef](#)]
19. Pramanik, A.K.; Harnagea, L.; Nacke, C.; Wolter, A.U.B.; Wurmehl, S.; Kataev, V.; Büchner, B. Fishtail effect and vortex dynamics in LiFeAs single crystals. *Phys. Rev. B* **2011**, *83*, 094502. [[CrossRef](#)]
20. Sundar, S.; Salem-Sugui, S.; Amorim, H.S.; Wen, H.H.; Yates, K.A.; Cohen, L.F.; Ghivelder, L. Plastic pinning replaces collective pinning as the second magnetization peak disappears in the pnictide superconductor $\text{Ba}_{0.75}\text{K}_{0.25}\text{Fe}_2\text{As}_2$. *Phys. Rev. B* **2017**, *95*, 134509. [[CrossRef](#)]
21. Taen, T.; Tsuchiya, Y.; Nakajima, Y.; Tamegai, T. Critical current densities and vortex dynamics in $\text{FeTe}_x\text{Se}_{1-x}$ single crystals. *Phys. C Supercond. Appl.* **2010**, *470*, 1106–1108. [[CrossRef](#)]
22. Ren, C.; Wang, Z.S.; Luo, H.Q.; Yang, H.; Shan, L.; Wen, H.H. Evidence for two energy gaps in superconducting $\text{Ba}_{0.6}\text{K}_{0.4}\text{Fe}_2\text{As}_2$ single crystals and the breakdown of the uemura plot. *Phys. Rev. Lett.* **2008**, *101*, 257006. [[CrossRef](#)] [[PubMed](#)]
23. Wang, X.L.; Dou, S.X.; Ren, Z.A.; Yi, W.; Li, Z.C.; Zhao, Z.X.; Lee, S.I. Unconventional superconductivity of $\text{NdFeAsO}_{0.82}\text{F}_{0.18}$ indicated by the low temperature dependence of the lower critical field H_{c1} . *J. Phys. Condens. Matter* **2009**, *21*, 205701. [[CrossRef](#)]
24. Martin, C.; Gordon, R.T.; Tanatar, M.A.; Kim, H.; Ni, N.; Bud'ko, S.L.; Canfield, P.C.; Luo, H.; Wen, H.H.; Wang, Z.; et al. Nonexponential London penetration depth of external magnetic fields in superconducting $\text{Ba}_{1-x}\text{K}_x\text{Fe}_2\text{As}_2$ single crystals. *Phys. Rev. B* **2009**, *80*, 020501. [[CrossRef](#)]
25. Abdel-Hafiez, M.; Ge, J.; Vasiliev, A.N.; Chareev, D.A.; Van De Vondel, J.; Moshchalkov, V.V.; Silhanek, A.V. Temperature dependence of lower critical field $H_{c1}(T)$ shows nodeless superconductivity in FeSe. *Phys. Rev. B* **2013**, *88*, 174512. [[CrossRef](#)]
26. Song, Y.J.; Ghim, J.S.; Yoon, J.H.; Lee, K.J.; Jung, M.H.; Ji, H.S.; Shim, J.H.; Bang, Y.; Kwon, Y.S. Small anisotropy of the lower critical field and the s_{\pm} -wave two-gap feature in single-crystal LiFeAs . *Europhys. Lett.* **2011**, *94*, 57008. [[CrossRef](#)]

27. Prozorov, R.; Kogan, V.G. London penetration depth in iron-based superconductors. *Rep. Prog. Phys.* **2011**, *74*, 124505–124525. [[CrossRef](#)]
28. Rosenstein, B.; Li, D. Ginzburg-Landau theory of type II superconductors in magnetic field. *Rev. Mod. Phys.* **2010**, *82*, 109–168. [[CrossRef](#)]
29. Tahara, S.; Anlage, S.M.; Halbritter, J.; Eom, C.B.; Fork, D.K.; Geballe, T.H.; Beasley, M.R. Critical currents, pinning, and edge barriers in narrow YBa₂Cu₃O_{7- δ} thin films. *Phys. Rev. B* **1990**, *41*, 11203–11208. [[CrossRef](#)] [[PubMed](#)]
30. Tinkham, M. *Introduction to Superconductivity*; Dover Publications: Mineola, NY, USA, 2004; ISBN 0486134725.
31. Arpaia, R.; Nawaz, S.; Lombardi, F.; Bauch, T. Improved nanopatterning for YBCO nanowires approaching the depairing current. *IEEE Trans. Appl. Supercond.* **2013**, *23*, 1101505. [[CrossRef](#)]
32. Wang, T.; Ma, Y.; Li, W.; Chu, J.; Wang, L.; Feng, J.; Xiao, H.; Li, Z.; Hu, T.; Liu, X.; et al. Two-gap superconductivity in CaFe_{0.88}Co_{0.12}AsF revealed by temperature dependence of the lower critical field $H_{c1}^c(T)$. *npj Quantum Mater.* **2019**, *4*, 33. [[CrossRef](#)]
33. Musolino, N.; Bals, S.; Van Tendeloo, G.; Clayton, N.; Walker, E.; Flükiger, R. Modulation-free phase in heavily Pb-doped (Bi,Pb)2212 crystals. *Phys. C Supercond. Its Appl.* **2003**, *399*, 1–7. [[CrossRef](#)]
34. Galluzzi, A.; Leo, A.; Masi, A.; Varsano, F.; Nigro, A.; Grimaldi, G.; Polichetti, M. Magnetic Vortex Phase Diagram for a Non-Optimized CaKFe₄As₄ Superconductor Presenting a Wide Vortex Liquid Region and an Ultra-High Upper Critical Field. *Appl. Sci.* **2023**, *13*, 884. [[CrossRef](#)]
35. Felner, I.; Kopelevich, Y. Magnetization measurement of a possible high-temperature superconducting state in amorphous carbon doped with sulfur. *Phys. Rev. B* **2009**, *79*, 233409. [[CrossRef](#)]
36. Yadav, C.S.; Paulose, P.L. Upper critical field, lower critical field and critical current density of FeTe_{0.60}Se_{0.40} single crystals. *New J. Phys.* **2009**, *11*, 103046. [[CrossRef](#)]
37. Stoner, E.C. XCVII. The demagnetizing factors for ellipsoids. *Lond. Edinb. Dublin Philos. Mag. J. Sci.* **1945**, *36*, 803–821. [[CrossRef](#)]
38. Prando, G.; Giraud, R.; Aswartham, S.; Vakaliuk, O.; Abdel-Hafiez, M.; Hess, C.; Wurmehl, S.; Wolter, A.U.B.; Büchner, B. Evidence for a vortex–glass transition in superconducting Ba(Fe_{0.9}Co_{0.1})₂As₂. *J. Phys. Condens. Matter* **2013**, *25*, 505701. [[CrossRef](#)] [[PubMed](#)]
39. Yeshurun, Y.; Malozemoff, A.P.; Shaulov, A. Magnetic relaxation in high-temperature superconductors. *Rev. Mod. Phys.* **1996**, *68*, 911–949. [[CrossRef](#)]
40. Maheshwari, P.K.; Gahtori, B.; Gupta, A.; Awana, V.P.S. Impact of Fe site Co substitution on superconductivity of Fe_{1-x}Co_xSe_{0.5}Te_{0.5} ($x = 0.0$ to 0.10): A flux free single crystal study. *AIP Adv.* **2017**, *7*, 15006. [[CrossRef](#)]
41. Murugesan, K.; Lingannan, G.; Ishigaki, K.; Uwatoko, Y.; Sekine, C.; Kawamura, Y.; Junichi, H.; Joseph, B.; Vajeeston, P.; Maheswari, P.K.; et al. Pressure Dependence of Superconducting Properties, Pinning Mechanism, and Crystal Structure of the Fe_{0.99}Mn_{0.01}Se_{0.5}Te_{0.5} Superconductor. *ACS Omega* **2021**, *6*, 30419–30431. [[CrossRef](#)] [[PubMed](#)]
42. Lei, H.; Hu, R.; Petrovic, C. Critical fields, thermally activated transport, and critical current density of β -FeSe single crystals. *Phys. Rev. B* **2011**, *84*, 014520. [[CrossRef](#)]
43. Dutta, P.; Pramanick, S.; Chatterjee, S. Effect of S-doping on the magnetic and electrical properties of FeSe superconductor. *Phys. C Supercond. Appl.* **2022**, *602*, 1354126. [[CrossRef](#)]
44. Fletcher, J.D.; Serafin, A.; Malone, L.; Analytis, J.G.; Chu, J.H.; Erickson, A.S.; Fisher, I.R.; Carrington, A. Evidence for a nodal-line superconducting state in LaFePO. *Phys. Rev. Lett.* **2009**, *102*, 147001. [[CrossRef](#)] [[PubMed](#)]
45. Takahashi, H.; Imai, Y.; Komiya, S.; Tsukada, I.; Maeda, A. Anomalous temperature dependence of the superfluid density caused by a dirty-to-clean crossover in superconducting FeSe_{0.4}Te_{0.6} single crystals. *Phys. Rev. B* **2011**, *84*, 132503. [[CrossRef](#)]
46. Bendele, M.; Weyeneth, S.; Puzniak, R.; Maisuradze, A.; Pomjakushina, E.; Conder, K.; Pomjakushin, V.; Luetkens, H.; Katrych, S.; Wisniewski, A.; et al. Anisotropic superconducting properties of single-crystalline FeSe_{0.5}Te_{0.5}. *Phys. Rev. B* **2010**, *81*, 224520. [[CrossRef](#)]
47. Milošević, M.V.; Perali, A. Emergent phenomena in multicomponent superconductivity: An introduction to the focus issue. *Supercond. Sci. Technol.* **2015**, *28*, 060201. [[CrossRef](#)]
48. Weyeneth, S.; Puzniak, R.; Mosele, U.; Zhigadlo, N.D.; Katrych, S.; Bukowski, Z.; Karpinski, J.; Kohout, S.; Roos, J.; Keller, H. Anisotropy of superconducting single crystal SmFeAsO_{0.8}F_{0.2} studied by torque magnetometry. *J. Supercond. Nov. Magn.* **2009**, *22*, 325–329. [[CrossRef](#)]
49. Gonnelli, R.S.; Daghero, D.; Tortello, M.; Ummarino, G.A.; Stepanov, V.A.; Kremer, R.K.; Kim, J.S.; Zhigadlo, N.D.; Karpinski, J. Point-contact Andreev-reflection spectroscopy in ReFeAsO_{1-x}F_x (Re = La, Sm): Possible evidence for two nodeless gaps. *Phys. C Supercond. Appl.* **2009**, *469*, 512–520. [[CrossRef](#)]
50. Szabó, P.; Pribulová, Z.; Pristáš, G.; Bud'ko, S.L.; Canfield, P.C.; Samuely, P. Evidence for two-gap superconductivity in Ba_{0.55}K_{0.45}Fe₂As₂ from directional point-contact Andreev-reflection spectroscopy. *Phys. Rev. B* **2009**, *79*, 012503. [[CrossRef](#)]
51. Mu, G.; Luo, H.; Wang, Z.; Shan, L.; Ren, C.; Wen, H.H. Low temperature specific heat of the hole-doped Ba_{0.6}K_{0.4}Fe₂As₂ single crystals. *Phys. Rev. B* **2009**, *79*, 174501. [[CrossRef](#)]
52. Bekaert, J.; Vercauteren, S.; Aperis, A.; Komendová, L.; Prozorov, R.; Partoens, B.; Milošević, M.V. Anisotropic type-I superconductivity and anomalous superfluid density in OsB₂. *Phys. Rev. B* **2016**, *94*, 144506. [[CrossRef](#)]
53. Klein, T.; Braithwaite, D.; Demuer, A.; Knafo, W.; Lapertot, G.; Marcenat, C.; Rodière, P.; Sheikin, I.; Strobel, P.; Sulpice, A.; et al. Thermodynamic phase diagram of Fe(Se_{0.5}Te_{0.5}) single crystals in fields up to 28 tesla. *Phys. Rev. B* **2010**, *82*, 184506. [[CrossRef](#)]

54. Diaconu, A.; Martin, C.; Hu, J.; Liu, T.; Qian, B.; Mao, Z.; Spinu, L. Possible nodal superconducting gap in $\text{Fe}_{1+y}(\text{Te}_{1-x}\text{Se}_x)$ single crystals from ultralow temperature penetration depth measurements. *Phys. Rev. B* **2013**, *88*, 104502. [[CrossRef](#)]
55. Kumar, R.; Varma, G.D. Study of TAFF and vortex phase of $\text{Fe}_x\text{Te}_{0.6}\text{OSe}_{0.40}$ ($0.970 \leq x \leq 1.030$) single crystals. *Phys. Scr.* **2020**, *95*, 045814. [[CrossRef](#)]
56. Poole, C.; Farach, H.; Creswick, R.; Prozorov, R. *Superconductivity*; Academic Press: Cambridge, MA, USA, 2007; ISBN 0080550487.
57. Peri, A.; Mangel, I.; Keren, A. Superconducting Stiffness and Coherence Length of $\text{FeSe}_{0.5}\text{Te}_{0.5}$ Measured in a Zero-Applied Field. *Condens. Matter* **2023**, *8*, 39. [[CrossRef](#)]
58. Bardeen, J. Critical fields and currents in superconductors. *Rev. Mod. Phys.* **1962**, *34*, 667–681. [[CrossRef](#)]
59. Maiorov, B.; Mele, P.; Baily, S.A.; Weigand, M.; Lin, S.Z.; Balakirev, F.F.; Matsumoto, K.; Nagayoshi, H.; Fujita, S.; Yoshida, Y.; et al. Inversion of the upper critical field anisotropy in FeTeS films. *Supercond. Sci. Technol.* **2014**, *27*, 044005. [[CrossRef](#)]
60. Her, J.L.; Kohama, Y.; Matsuda, Y.H.; Kindo, K.; Yang, W.H.; Chareev, D.A.; Mitrofanova, E.S.; Volkova, O.S.; Vasiliev, A.N.; Lin, J.Y. Anisotropy in the upper critical field of FeSe and $\text{FeSe}_{0.33}\text{Te}_{0.67}$ single crystals. *Supercond. Sci. Technol.* **2015**, *28*, 045013. [[CrossRef](#)]
61. Sun, Y.; Pan, Y.; Zhou, N.; Xing, X.; Shi, Z.; Wang, J.; Zhu, Z.; Sugimoto, A.; Ekino, T.; Tamegai, T.; et al. Comparative study of superconducting and normal-state anisotropy in $\text{Fe}_{1+y}\text{Te}_{0.6}\text{Se}_{0.4}$ superconductors with controlled amounts of interstitial excess Fe. *Phys. Rev. B* **2021**, *103*, 224506. [[CrossRef](#)]
62. Mishev, V.; Nakajima, M.; Eisaki, H.; Eisterer, M. Effects of introducing isotropic artificial defects on the superconducting properties of differently doped Ba-122 based single crystals. *Sci. Rep.* **2016**, *6*, 27783. [[CrossRef](#)] [[PubMed](#)]
63. Kondo, K.; Motoki, S.; Hatano, T.; Urata, T.; Iida, K.; Ikuta, H. $\text{NdFeAs}(\text{O,H})$ epitaxial thin films with high critical current density. *Supercond. Sci. Technol.* **2020**, *33*, 09LT01. [[CrossRef](#)]
64. Li, J.; Yuan, J.; Yuan, Y.H.; Ge, J.Y.; Li, M.Y.; Feng, H.L.; Pereira, P.J.; Ishii, A.; Hatano, T.; Silhanek, A.V.; et al. Direct observation of the depairing current density in single-crystalline $\text{Ba}_{0.5}\text{K}_{0.5}\text{Fe}_2\text{As}_2$ microbridge with nanoscale thickness. *Appl. Phys. Lett.* **2013**, *103*, 62603. [[CrossRef](#)]
65. Bristow, M.; Knafo, W.; Reiss, P.; Meier, W.; Canfield, P.C.; Blundell, S.J.; Coldea, A.I. Competing pairing interactions responsible for the large upper critical field in a stoichiometric iron-based superconductor $\text{CaKFe}_4\text{As}_4$. *Phys. Rev. B* **2020**, *101*, 134502. [[CrossRef](#)]
66. Sun, Y.; Ohnuma, H.; Ayukawa, S.-Y.; Noji, T.; Koike, Y.; Tamegai, T.; Kitano, H. Achieving the depairing limit along the c axis in $\text{Fe}_{1+y}\text{Te}_{1-x}\text{Se}_x$ single crystals. *Phys. Rev. B* **2020**, *101*, 134516. [[CrossRef](#)]
67. Galluzzi, A.; Buchkov, K.; Tomov, V.; Nazarova, E.; Kovacheva, D.; Leo, A.; Grimaldi, G.; Pace, S.; Polichetti, M. Mixed state properties of iron based $\text{Fe}(\text{Se,Te})$ superconductor fabricated by Bridgman and by self-flux methods. *J. Appl. Phys.* **2018**, *123*, 233904. [[CrossRef](#)]
68. Tsurkan, V.; Deisenhofer, J.; Günther, A.; Kant, C.; Klemm, M.; von Nidda, H.-A.; Schrettle, F.; Loidl, A. Physical properties of $\text{FeSe}_{0.5}\text{Te}_{0.5}$ single crystals grown under different conditions. *Eur. Phys. J. B* **2011**, *79*, 289–299. [[CrossRef](#)]
69. Wittlin, A.; Aleshkevych, P.; Przybylińska, H.; Gawryluk, D.J.; Dłuzewski, P.; Berkowski, M.; Puźniak, R.; Gutowska, M.U.; Wiśniewski, A. Microstructural magnetic phases in superconducting $\text{FeTe}_{0.65}\text{Se}_{0.35}$. *Supercond. Sci. Technol.* **2012**, *25*, 065019. [[CrossRef](#)]
70. Sivakov, A.G.; Bondarenko, S.I.; Prokhvatilov, A.I.; Timofeev, V.P.; Pokhila, A.S.; Koverya, V.P.; Dudar, I.S.; Link, S.I.; Legchenkova, I.V.; Bludov, A.N.; et al. Microstructural and transport properties of superconducting $\text{FeTe}_{0.65}\text{Se}_{0.35}$ crystals. *Supercond. Sci. Technol.* **2017**, *30*, 015018. [[CrossRef](#)]
71. McQueen, T.M.; Huang, Q.; Ksenofontov, V.; Felser, C.; Xu, Q.; Zandbergen, H.; Hor, Y.S.; Allred, J.; Williams, A.J.; Qu, D.; et al. Extreme sensitivity of superconductivity to stoichiometry in Fe_{1+y}Se . *Phys. Rev. B* **2009**, *79*, 014522. [[CrossRef](#)]
72. Onar, K.; Yakinci, M.E. Solid state synthesis and characterization of bulk β - FeSe superconductors. *J. Alloys Compd.* **2015**, *620*, 210–216. [[CrossRef](#)]
73. Fiamozzi Zignani, C.; De Marzi, G.; Grimaldi, G.; Leo, A.; Guarino, A.; Vannozzi, A.; della Corte, A.; Pace, S. Fabrication and Physical Properties of Polycrystalline Iron-Chalcogenides Superconductors. *IEEE Trans. Appl. Supercond.* **2017**, *27*, 1–5. [[CrossRef](#)]
74. Galluzzi, A.; Nigro, A.; Fittipaldi, R.; Guarino, A.; Pace, S.; Polichetti, M. DC magnetic characterization and pinning analysis on $\text{Nd}_{1.85}\text{Ce}_{0.15}\text{CuO}_4$ cuprate superconductor. *J. Magn. Magn. Mater.* **2019**, *475*, 125–129. [[CrossRef](#)]
75. Galluzzi, A.; Mancusi, D.; Cirillo, C.; Attanasio, C.; Pace, S.; Polichetti, M. Determination of the Transition Temperature of a Weak Ferromagnetic Thin Film by Means of an Evolution of the Method Based on the Arrott Plots. *J. Supercond. Nov. Magn.* **2018**, *31*, 1127–1132. [[CrossRef](#)]

Disclaimer/Publisher’s Note: The statements, opinions and data contained in all publications are solely those of the individual author(s) and contributor(s) and not of MDPI and/or the editor(s). MDPI and/or the editor(s) disclaim responsibility for any injury to people or property resulting from any ideas, methods, instructions or products referred to in the content.